Published in final edited form as:
Phys Med Biol. 2012 July 7; 57(13): 4403–4424. doi:10.1088/0031-9155/57/13/4403.

A nephron-based model of the kidneys for macro-to-micro α-particle dosimetry

Robert F Hobbs[1], **Hong Song**[1], **David L Huso**[2], **Margaret Sundel**[1], and **George Sgouros**[1]
[1]Department of Radiology, Johns Hopkins University, Baltimore MD, USA

[2]Department of Comparative Pathology, Johns Hopkins University, Baltimore MD, USA

Abstract

Objective—Targeted α-particle therapy is a promising treatment modality for cancer. Due to the short path-length of α-particles, the potential efficacy and toxicity of these agents is best evaluated by microscale dosimetry calculations instead of whole-organ, absorbed fraction –based dosimetry. Yet time-integrated activity (TIA), the necessary input for dosimetry, can still only be quantified reliably at the organ or macroscopic level. We describe a nephron- and cellular-based kidney dosimetry model for α-particle radiopharmaceutical therapy, more suited to the short range and high linear energy transfer of α-particle emitters, which takes as input kidney or cortex TIA and through a macro to micro model-based methodology assigns TIA to micro-level kidney substructures. We apply the model to provide nephron-level S-values for a range of isotopes allowing for pre-clinical and clinical applications according to the medical internal radiation dosimetry (MIRD) schema.

Methods—We assume that the relationship between whole-organ TIA and TIA apportioned to microscale substructures as measured in an appropriate pre-clinical mammalian model also applies to the human. In both, the pre-clinical and the human model, microscale substructures are described as a collection of simple geometrical shapes akin go those used in the Cristy-Eckermann phantoms for normal organs. Anatomical parameters are taken from the literature for a human model, while murine parameters are measured, *ex vivo*. The murine histological slides also provide the data for volume of occupancy of the different compartments of the nephron in the kidney: glomerulus vs. proximal tubule vs. distal tubule. Monte Carlo simulations are run with activity placed in the different nephron compartments for several α-particle emitters currently under investigation in radiopharmaceutical therapy.

Results—The S-values were calculated for the α-emitters and their descendants between the different nephron compartments for both the human and murine models. The renal cortex and medulla S-values were also calculated and the results compared to traditional absorbed fraction calculations.

Conclusions—The nephron model enables a more optimal implementation of treatment and is a critical step in understanding toxicity for human translation of targeted α-particle therapy. The S-values established here will enable a MIRD-type application of α-particle dosimetry for α-emitters, i.e.: measuring the time-integrated activity in the kidney (or renal cortex) will provide meaningful and accurate nephron-level dosimetry.

Corresponding author: Robert F Hobbs, PhD, Department of Radiology, Johns Hopkins University, School of Medicine, CRB II 4M.60, 1550 Orleans St., Baltimore MD 21231, rhobbs3@jhmi.edu, Phone: 410-502-8185 Fax: 413-487-3753.

I. INTRODUCTION

Current cancer treatment is rarely effective once the tumor has metastasized to distant sites. The eradication of such metastases requires a systemic, targeted therapy that is minimally susceptible to chemo- or radio-resistance, that is potent enough to sterilize individual tumor cells and cell clusters and that exhibits an acceptable toxicity. Alpha-particle emitting radionuclides are being investigated as possible cytotoxic agents (1, 2). Alphas are highly effective (1–3 α-particle tracks can sterilize a cell, as opposed to the thousands of tracks necessary from β-particles), are not susceptible to chemoresistance, and are minimally susceptible to radioresistance (3). Consequently, there is growing interest in α-particle emitters for cancer therapy. Pre-clinical and clinical investigation of α-emitters has highlighted the need for micro-scale dosimetry calculations applicable to normal organ geometries (4–6). More specifically, early α-emitter studies using ^{211}At (7, 8), and later studies with ^{213}Bi (9, 10), ^{225}Ac (4) and ^{223}Ra (11–13) have evolved into clinical trials, specifically, ^{211}At therapy of ovarian cancer (14) and glioblastoma (15, 16) as well as ^{213}Bi and ^{225}Ac therapy of leukemia (17, 18), ^{213}Bi therapy of glioblastoma (19), and ^{223}Ra therapy of bone metastases in prostate cancer patients, all with promising results.

The absorbed dose is equal to the energy imparted to a target divided by the target mass. The energy imparted to a target depends upon the radionclide's emission spectrum and the anatomical distribution of emitters. The Medical Internal Radiation Dose (MIRD) Committee established a schema to facilitate dosimetry calculations in nuclear medicine (20, 21). The basic equation is:

$$D_t = \sum_s \frac{\tilde{A}_s \cdot \Delta \cdot \phi_{t \leftarrow s}}{m_t}. \quad (1)$$

That is, the absorbed dose in a target region, D_t, (usually an organ) is equal to the sum of the dose contributions from all sources in the body. Each contribution is equal to the time integrated activity (number of radionuclide transformations), $\tilde{A}_s$, in the source multiplied by the energy per transformation, Δ, (isotope dependent) multiplied by the fraction of emitted energy, $\phi_{t \leftarrow s}$, that originates in the source (organ) and is absorbed by the target (organ), divided by the target mass, m_t.

In this formalism, a series of first order idealized "standard" anthropomorphic phantom models (developed by Cristy and Eckerman (22) from simple geometrical shapes) were used to represent the various normal organs. Thus m_t and $\phi_{t \leftarrow s}$ are constants relative to a specific model. Moreover, Δ is constant for each isotope. Accordingly, the TIA-independent portion of equation (1) was compiled as a set of phantom and radionuclide-dependent "S-values" (20, 23):

$$D_t = \sum_s \tilde{A}_s \cdot S_{t \leftarrow s} \quad (2)$$

As currently implemented, the fundamental assumption in this "absorbed fraction" approach is of a uniform distribution of emitters in the source volume and a calculation that gives the average absorbed dose to the target volume. In principle, the formalism applies also to highly non-uniform activity and dose distributions, however, when the necessary delineation for accurate dosimetry within this framework fails to correlate with functional unit or sub-unit anatomy, it becomes difficult to determine what *a priori* volume distinctions need to be made. The emergence of α-emitters in radiopharmaceutical therapy, in particular, whose range is on the order of 50–80 μm, highlights the need to develop alternative approaches and

models that can accommodate the substantially smaller scale needed to relate absorbed dose to biological effects with these agents. In such cases, the information needed is on a scale that is substantially smaller than: (a) the resolving power of clinical imaging detectors and modalities, and (b) the scale of human organs.

In such scenarios, the MIRD committee (24), along with others (2, 25) have recommended cell-level and microdosimetry calculations that are based on *a priori* bio-distribution information obtained from pre-clinical or, when the sub-cellular distribution is also relevant, cell-based studies. Such cell-level and microdosimetric approaches have been implemented for laboratory animal *ex vivo* and cellular *in vitro* studies (12, 26–28), including most recently an S-value methodology applied to the testes (29). However, for such approaches to be applicable clinically, an accompanying method for assigning activity or time-integrated activity distributions measured on a macroscopic scale to microscopic dimensions using pre-clinical studies to relate the macro measurements to micro distributions is necessary. Application to human dosimetry then requires that the assumed macro to micro correspondence is species-independent.

Using ^{225}Ac we have previously investigated antibody-targeted therapy against breast cancer metastases (4). In these studies, control mice survived with a median duration of 40 days, while 8/12, ^{225}Ac-Ab-treated mice exhibited long-term (>1 year) asymptomatic survival. At necropsy, however, these mice showed signs of radiation-induced renal pathology. The averaged kidney and renal cortex absorbed doses calculated from these studies were well below the threshold expected for renal toxicity (4, 5). This discrepancy demonstrates that the average absorbed dose over the macroscopic kidney or renal cortex volume fails to predict biological consequences that most likely arise because the microdistribution of the α-emitter and therefore the dose distribution is not uniformly distributed in the relevant target volume. Studies have been undertaken to characterize the localization of various radiopharmaceuticals to the different compartments most susceptible to toxicity (identified as the proximal tubules and glomeruli) (14, 30–34). The damage to the proximal tubules and glomeruli are described with detail, including concessions that such damage is greater than expected from absorbed fraction dose calculations; however, to date no systematic methodology or methodological extension exists for dose quantification at the sub-cortex level.

II. METHODS

Approach

The nephron and its constituent components and cells have dimensions on the scale of α-particle decay ranges. A nephron-based model can, therefore, be defined to provide values according to the MIRD formalism (Eq 2). However, there are a few important distinctions to consider while developing this model:

1. The nephron is not unique (or a pair), unlike the Cristy-Eckerman phantom compartments, which are organ-based (22). There are an average of 600,000 nephrons in a human kidney (35). The nephron model is representative of a large number of similar, though not identical entities. However, the MIRD formalism and the phantoms are also representative rather than exact for each individual. As such the use of a single average nephron does not represent a large deviation from the established formalism, as long as the proper conversion of the S-values established in the individual nephron are scaled correctly to the whole compartments.
2. Activity (and consequently the time-integrated activity (TIA), $\tilde{A}_i$) is not directly obtainable through imaging in the nephron compartments, but can only be

measured *ex vivo*. Therefore a mechanism which enables the translation of measured activity (and TIA) in the kidney or renal cortex to the activity (and TIA) in the different nephron compartments is required for the model. This macro to micro translational mechanism must be established in an appropriate pre-clinical model; in this work we have used a murine model. Once established, the approach can also be implemented to convert human macroscopic activity and TIA measurements to levels that can be defined at the microscopic scale in humans, given basic anatomical parameters for human kidneys. This procedure is described in greater detail in the macro to micro section, below. Once the macroscopically measured TIA is apportioned to the microscale compartments microscale S values may be used to calculate the absorbed dose. S values are obtained by Monte Carlo simulations as described below.

Monte Carlo Simulations

Monte Carlo (MC) simulations were performed using GEANT4 version 9.2. GEANT4 is a general-purpose MC code that simulates the transport of several particle types in a wide range of energies (36). It was originally developed for simulating high energy physics experiments, but is becoming increasingly popular in the field of medical physics, often as GATE4. GEANT4 modeling has been successfully applied to radiopharmaceutical therapy (RPT) dosimetry, either as a complement to direct clinical measurements (37) or to investigate cellular level dosimetry (25, 38). It has also already been validated and used for α-particle dosimetry (25, 39, 40). More specifically, GEANT4 α-particle modeling has been validated by comparison to MCNPX (40). The continuous energy losses along the track of the α-particle range are modeled by the Bethe-Bloch equation, which is modified by taking into account various corrections including multiple scattering of charged particles as well as knock-on electron (delta ray) production, which was implemented by lowering the distance threshold for electron tracking to 1 nm. Source to target S-value calculations were performed by simulating 100,000 decays in the source volume and tallying their energy deposition in the target volume.

Anatomical Nephron

The functional sub-unit of the kidney is the nephron, composed of the glomerulus and its associated microvasculature, collectively known as Bowman's capsule, and the tubules. The glomerulus filters the blood and the filtrate then passes through the tubules before exiting the kidney through the collecting ducts. The initial portion of the tubule, the proximal tubule is convoluted; the proximal tubule then extends from the cortex in to the medulla and returns in a loop known as the loop of Henle. The character of the tubule changes during this descent and becomes the distal tubule. The proximal tubule is the region where the free metalloids are most likely to be absorbed (41); together with the glomerulus, they are the regions which exhibit toxicity in murine studies of renal toxicity due to ^{225}Ac or ^{211}At therapy (30, 31, 33, 42), therefore the modeled version of the nephron focuses on these two sub-units.

Idealized Model

The simplest form of the idealized nephron model uses 3-dimensional geometrical shapes (cylinders, spheres and toroids), as illustrated in figure 1, which shows the development of the model. The glomerulus was modeled as a simple sphere, the proximal tubules as three hollow cylinders and connecting toroids through which the fluid to be filtered is passed (side view, top left corner), originally all centered in the x-z plane. The third proximal tubule was then folded upon itself for compactness (top view, top right corner) by rotating the third tubule around an axis parallel to the z-axis and centered on the second tubule. This rotation is denoted as R(θ) in the figure with $\theta = 2\pi/3$. The three cylinders in this view are seen as

circles; they have thicker outlines to identify them more easily. Next, the radius of curvature, r_C, used for the toroids is reduced to the radius of the tubules, r_t, plus a small margin $\varepsilon = 1$ μm, this is illustrated by the two converging arrows at the bottom of the sub-figure showing the reduction of the torus radius rc to a value close to the tubule radius, $r_c \rightarrow r_t + \varepsilon$. This result of this operation is to bring cylinders together as seen in the bottom right corner of the figure where the three cylinders are now represented by the central three thick circles. At his point the models used in the MC departed from the whole nephron model and the tubules were separated from the glomerulus due to the necessity of considering external contributions and optimizing the models to represent the average contributions from all sources as befits an S-value calculation. The tubule portion of the model has only three tubule folds, but since the range of the α-particles is larger than the tubule radius, nearest neighbor tubules must be taken into account in the MC. This is also illustrated in the lower right corner of the figure where a cross-section of the three tubule folds is shown, which comprise the target volume, along with the neighboring tubules within range of the α-emissions. Some of these neighbor tubules will be distal and the ratio of distal versus proximal tubule neighbors is modeled based on the respective measured fractions of occupancy in the murine renal cortex. Since this percentage is based on a cortex-wide occupancy, these nearest neighbors could or could not be part of the same anatomical nephron in the kidney without consequence to the MC since activity will be placed according to concentration in all source (proximal) tubules within range of the three target tubules. The tubule (and glomerulus) has been subdivided into individual cells as seen in the blow-up in the bottom left corner of figure 1. For the tubule, these consist of simple cuboidal epithelial cells. However, although the nuclei are represented, no attempt was made to distinguish between the cytoplasm and the nucleus in the simulations. For the tubules, different sources were considered: activity in the proximal renal tubule cells (prtc), activity on the proximal renal tubule luminal surface (prts), and activity within the lumen (prtl). as well as the contribution from activity in the glomerulus. To calculate S-values, the activity within the different sources was distributed randomly and the energy collected in the target tubule cells; here however, the cellular division played no significant role, as the target mass considered was the entirety of the three tubules.

For the glomerulus both as a source for dose contributions to the tubules and as a target, a simple sphere was used along with a similar procedure to determine the contribution to and from surrounding tissue and compartments (not shown). However, while the fraction of occupancy of proximal versus distal tubule cells in the surrounding volume was attributed in the same manner, the relative geometry of the tubule sub-structure (cells versus lumina) with respect to the glomeruli was less clear and could not be modeled with any pretense of accuracy. Therefore the tissue surrounding the glomerulus was modeled as a whole and as a single source and target (prt). The results between glomerulus and tubule were then scaled to the relative occupancy of the source organ (glomerulus or tubule).

Murine model

The idealized geometrical models have been adapted to the mouse using anatomical parameters measured *ex vivo*. Figure 2 shows a cross-section of a mouse kidney which was stained with periodic acid Schiff (PAS) stain. PAS positive material shows up along the brush border (lumen surface) of the proximal tubules (examples contoured in blue, distal tubules shown in red). The glomeruli are easily distinguishable and shown contoured in green. The average (a) lumen, (b) proximal tubule and (c) glomeruli diameters were measured from random samples of 50 different mouse kidney slices, cut transverse to the cortex geometry, using a Nikon 80i microscope at 10x magnification and the accompanying NIS-Elements BL software and used in the idealized phantom. Once a glomerulus was identified for measurement, the diameter was measured in the slice where the glomerulus was largest; care was taken not to duplicate glomerular measurements, i.e.: the sampling was

random, but with a constraint not to measure in the same location for a spacing of at least three slides.

Alpha emitters in use in RPT

The α-emitters currently in use in clinical RPT trial or pre-clinical experiments consist of: ^{211}At, ^{225}Ac, ^{213}Bi, ^{227}Th, ^{223}Ra, ^{212}Pb and ^{212}Bi. The decay chains of these radioisotopes are illustrated in figure 3, while the energy per decay and branching ratios of the decay chains are also provided in table I (43). From these it can be seen that ^{213}Bi is a descendant of ^{225}Ac, ^{223}Ra is a descendant of ^{227}Th and ^{212}Bi is a descendant of ^{212}Pb, which is itself technically speaking, not an α-emitter. In addition to the descendants used in therapy, certain other descendants have a sufficiently long half-life to potentially enable re-localization before further decay. This is the case for ^{221}Fr, ^{211}Pb and ^{211}Bi, for example. Therefore, S-values for these intermediate descendants are calculated separately from the S-values of the original parent radionuclides and are indicated by a change in color in figure 3. The S-value contributions of short-lived (< 1 min) descendants are included in the S-values of the original parent isotope and are shown in the same color in figure 3.

The β-particle decays in the decay chains (shown in black in figure 3) are not adequately represented using the nephron model. The range of energy deposition is substantially longer than the scale of the nephron and so only a fraction of the energy emitted is absorbed in the same nephron. Most of the β-particle energy absorbed in an individual nephron will be from other nephrons. Therefore the absorbed dose from β-particles should be calculated using the whole kidney model (44) and the energy from β decays is not included in any parent α-particle S-value. For the murine cases, Monte Carlo calculations were run using the MIRD 19 parameters (44) scaled to average mouse kidney mass (300 mg). The human β-particle S-values are available in OLINDA/EXM (45) or from MIRD publications (46). As noted in MIRD Pamphlet 22, dosimetry calculations involving α-emitters should separately report the absorbed dose from α-particles and low LET emissions such as electrons or photons as these have a different relative biological effectiveness adjustment.

Compartmental S-values

Re-writing equation (2) for the kidney, the dose to a target compartment, D_{tc}, may be written as:

$$D_{tc} = \sum_{sc} S_{tc \leftarrow sc} \cdot \tilde{A}_{sc} \quad (3)$$

In this equation, a distinction is made between kidney glomeruli or proximal tubules, (considered as a compartment of the kidneys and used collectively as a target (tc) or source (sc) volume), and the individual or unit source (su) or target (tu) volume which is the glomerulus or the tubule as defined in the nephron model used for the MC calculations. In order to exploit equation (3), a relationship between the unknown compartment S-value and the simulated Monte Carlo unit S-value, $S_{tu \leftarrow su}$, must be found. The S-value may be derived from equations (1) and (2):

$$S_{t \leftarrow s} = \frac{\Delta \cdot \phi_{t \leftarrow s}}{m_t} \quad (4)$$

This equation may be written for both the compartment and unit S-values; since Δ is constant and, for a given source-target combination, ϕ is also constant, one can solve for the Δϕ product in one version (compartment or unit) of equation (4) and substitute the value into the other version of the equation to obtain:

$$S_{tc\leftarrow sc}=S_{tu\leftarrow su}\frac{m_{su}}{m_k\cdot f_c} \quad (5)$$

where m_{su} is the mass of the source volume used in the unit nephron model and the denominator in equation (5) is the mass of the corresponding kidney compartment, which is the mass of the kidney, m_k multiplied by the fraction of occupancy of the compartment, f_c

The fractions of occupancy of the tubules and glomeruli were measured in the murine model by stitching together the histological slides using the Nikon Elements BL software into images of whole kidney slices (figure 4) and by identifying and delimiting the different components. Specifically, a mouse kidney was extracted and sliced lengthwise every 15 μm across the entire kidney; images were taken of the slides and stitched together using the NIS Elements software (figure 4). Every third slice was sampled from the exterior slice through to the midpoint slice (total of 26) in order to obtain a representative sampling. Contours were drawn on randomly determined regions from all slices delineating the kidney into cortex vs. medulla/pelvis sub-sections as well as glomerulus vs. proximal tubule vs. distal tubule vs. other sub-sections. Note that although the fractions of occupancy, f_c were measured in mice, they were also applied to the human model; corresponding measurements could be performed in humans, from cadavers (47) or surgical samples (48).

Once the fractions were determined, the whole compartment S-values were calculated using equation (5) and the Monte Carlo unit S-values. Note that since the contributions from the neighboring tubules were not assumed to be part of the same nephron, cross-fire between nephrons is accounted for in the unit S value calculations.

Macro to micro (e.g., kidney to nephron) modeling

While the rationale for S-values for microscopic structures is compelling, its clinical utility is not evident: after all, activity cannot be measured in individual nephrons *in vivo*. The activity is measured clinically at the level of the kidney, or at best, the renal cortex. Therefore, a mechanism is necessary which will enable the translation of TIA measured in the kidney (or cortex, the macro scale) to the TIA to be entered into equation (2) using the collective nephron compartment (the micro scale) in order for this methodology to be applicable clinically. The kidney TIA, $\tilde{A}_k$, may be expressed as:

$$\tilde{A}_k=\sum_{sc,i}\tilde{A}_{sc,i}=\sum_{sc,i}g_{sc,i}\tilde{A}_k \quad (6)$$

that is, it is the sum of the TIAs in the different source compartments (sc), which can be expressed as fractions ($g_{sc,i}$) of the kidney TIA, where i is the summation index for the different contributing isotopes within the parent decay chain, since long-lived descendants may relocate and contribute dose to different organs and compartments. Combining this equation with equation (3) yields:

$$D_{tc}=\sum_{sc,i}S_{tc\leftarrow sc,i}\cdot g_{sc,i}\cdot\tilde{A}_k \quad (7)$$

The dosimetric quantity of interest, D_{tc}, is now expressed as a function of the measurable kidney TIA, $\tilde{A}_k$. Equation (7) is the equation which will be used to apply the model presented in this paper. However, in order to exploit this formalism, the $g_{sc,i}$ values must be established. These values are in principle specific to each radiopharmaceutical, that is to a specific targeting agent (antibody, peptide, etc) – α-emitter combination. While the establishment of a library of such values is beyond the scope of this paper, a method for the

measurement and calculation of $g_{sc,i}$ is described. The definition of $g_{sc,i}$ as a ratio of compartment TIA to kidney TIA in equation (6) is the basis of the method and as defined would require the measurement of compartment TIA which must be measured *ex vivo*, and therefore in mice. Because the relative activities may change over time due to the specific pharmacokinetics, the TIA ratio parameters, $g_{sc,i}$, should be established using the necessary number of time points, similar to the establishment of TIA for input in traditional MIRD methodology. This principle is illustrated in figure 5 for a single contributing isotope and represents equation (6). The assumption in the present model is that only two compartments contribute significantly to renal toxicity and require measurement: the proximal tubules and the glomeruli. Note that for a real kidney the sum of the compartment activities will not exactly equal the total activity as there are more compartments present, particularly at earlier times. Depending upon the agent and its micro-scale distribution within the kidneys, at later times, the contribution of activities from other compartments is expected to be minimal.

An additional complication is that the activity over time, and therefore, the TIA, cannot realistically be measured for each tubule and glomerulus that collectively make up the target or source compartment activities; however, by measuring the activity in a small number of sampled identifiable compartment volumes, the activity concentration, $c_{sc,i}(t)$, i.e.: the activity per unit volume, and by extension, the time integrated activity concentration, $\tilde{c}_{sc,i}$, can be measured (34). Re-scaling equation (6) to activity concentrations gives:

$$g_{sc,i} = \frac{\tilde{c}_{sc,i} \cdot f_c}{\tilde{c}_k} \quad (8)$$

where f_c is the fraction of occupancy of the source compartment. Once the $g_{sc,i}$ values are established for the specific radiopharmaceutical, the dose to the compartments may be established using equation (7) and external methods of measuring kidney TIA. Note that all the formalism developed here has been described for the kidney; the renal cortex may be substituted *in lieu* of the kidney with equal validity as long as it is done in a consistent manner.

III. RESULTS

Anatomical parameters

The human model used parameters taken from the literature (49); these are 23 μm for the epithelial cell (proximal tubule wall) thickness and 33 μm for the tubule lumen radius. The glomerulus radius used was 150 μm. The corresponding parameters for the murine nephron model were measured directly from the identified anatomical features in 50 different kidneys slices from 5 FVB/N strain mice (derived from an outbred Swiss strain (50)). The average and root mean square values were (28 +/− 8) μm for the proximal tubule diameter, (10 +/− 3) μm for the tubule lumen diameter, and (65 +/−20) μm for the glomerulus diameter. These values compare favorably to those found in the literature, where a value of 33 μm for the glomerular diameter is reported for 10 week old mice (51). The average values were used in the Monte Carlo calculation.

S-values

S-values were calculated for both the murine and human nephron models for the isotopes shown in figure 3, by collecting the deposited energy in the different target compartments and dividing by the target mass. The S-values (both for the unit model and the converted compartmental values) are given in tables IIa–IIh using the murine parameters and tables IIIa–IIIh for the human model for all α-emitters which includes the short-lived (<1 min) α-emitting descendants designated with the same color in figure 3. Additionally, the energy

per decay corresponding to the S-value is provided as well as the percentage of the kinetic energy of the α-particle (compared to values in table I) deposited in the target volume. The target volumes are the glomerular cells (glc) and the proximal tubule cells (prtc), while the source compartments include the target volumes as well as the proximal tubule lumina (prtl) and the inner surface of the proximal tubule cells (prts) for the proximal tubule cells. The relative geometry of the tubules with respect to the glomeruli is not well defined, therefore, a single, average or representative, proximal tubule component (prt) was considered for the glomerulus. The S-values for the macroscopic compartments, the kidney (kid) and cortex (cor) are also provided for comparison. The β-particle S-values and energy per decay for the kidney and cortex in the murine model are provided in tables IVa–IVc. The results show that for the murine model the assumption of 100 % local deposition from β-emitters even at the level of the kidney or the cortex can lead to a significant overestimation of dose, depending on the energy of the β-decays. Note that the half-life of ^{207}Bi is 31.6 years, therefore the decays were not taken into consideration as contributing to the absorbed dose; consequently, the decay is represented by a squiggly line in figure 3a rather than a straight line.

Fractions of occupancy

The conversion of the Monte Carlo S-values to whole compartment S-values depends upon the percentage of volume (fraction of occupancy, f_C) allocated in the kidney to the critical sub-units (proximal tubules and glomeruli). From the sampling measurements of the histological slides, it was determined that the proximal tubules occupy 81 % of the cortex, or equivalently 53 % of kidney. The proximal tubule cells, i.e.: the tubules without the lumina, occupy 66 % and 43 % of the cortex and kidney, respectively, while the glomeruli occupy 2.3 % of the cortex and 1.5 % of the kidney. A value of 80 % was used in determining the fraction of nearest neighbor tubules to be proximal as opposed to distal for both the glomerulus and proximal tubule targets in the Monte Carlo calculation.

IV. DISCUSSION

Absorbed dose and the dose-rate-dependent radiobiologically derived quantity biologic effective dose have been shown to correlate with normal organ toxicity (52, 53); therefore the accurate calculation of these quantities is essential to provide optimal personalized therapy regimens for patients. Targeted α-emitter therapy holds great promise as a cancer treatment but also comes with a potential for toxicity. Understanding and correctly implementing the absorbed dose calculations to normal organs at risk is critical in encountering unexpected toxicity or implementing a sub-optimal treatment strategy.

Measurement of input parameters

The model assumes that two of the input values in equation (6) can be measured with accuracy:

1. the first is the parameter $g_{sc,i}$, which must be established for each different radiopharmaceutical. In order to do so activity must be measured at the nephron level ex *vivo*. Even so, accurate quantification remains a challenge when distinguishing between different compartments. While different options are available, including autoradiography, the α-Camera, recently invented by Bäck et al. (34) holds the most promise as a modality capable of achieving the requisite accuracy. By taking into consideration the different half-lives of the different contributing isotope decays, measuring the activity at multiple time points and fitting the results to the appropriate exponential functions, activity from the different contributors can be distinguished (4).

2. The traditional input, $\tilde{A}_k$, to the absorbed fraction methodology, which assumes that activity can be measured with external patient imaging such as SPECT. This also assumes that the α-decays are accompanied by photon emissions, which is usually the case, but the administered activity in some cases may be below camera sensitivity. In such cases, pre-treatment tracer studies using surrogate photon-emitting radionuclides may be collected. In the case of several isotopes, notably ^{225}Ac, α-emitting descendants are a main concern for toxicity, and the contribution to the absorbed doses from the different radionuclides must be taken into account (4, 32). Therefore the method and quantification must be applied to all isotopes with the potential to relocate, which also means possibly imaging with different energy windows in order to distinguish between different isotope activities, or imaging repeatedly over the range of half-lives and fitting the activity curves to the appropriate exponential equations (4).

S-values and model compartments

Although no direct experimental validation of the model is provided, the accompanying energy per decay and percentage values provided in tables II, III and IV are consistent with expectations. The differences in the S-values between the different proximal tubule sources (tubule cells, tubule surface, tubule lumen) to the tubule cells are minimal and can be expected to be below uncertainties for the murine model. For the human model, the differences become more important, therefore more accurate dosimetry will be obtained by apportioning the TIA appropriately into the different proximal tubule source regions. Depending on the accuracy of the quantification for $g_{sc,i}$ determination the investigator may have to either assume localization based on bio-chemical, *a priori*, knowledge or assign the TIA to the cell compartment which would maximized the calculated dose and therefore err on the side of safety.

In principle, a further delineation of source and target regions is possible within the glomerulus, however, because the scale of the sub-structure is small and relatively homogenous even on the scale of α-emissions, initial studies showed no significant differences in results from different localization of activity within the glomerulus. Similarly, in future extensions, as circumstances dictate, the glomerulus could be expanded as a Bowman's capsule and include the microvasculature. The model does not take into account possible differentiation of uptake between superficial and juxtamedullary nephrons (54); should future experiments and circumstances dictate, the model would have to be refined in this direction.

Human model

Since it is not possible to measure activity distribution, in humans, at the level of detail required to implement the S-values calculated in this work, the TIA obtained from macroscopic measurements must be apportioned to the appropriate microscopic structure using the values derived from the mouse model. By assuming that the apportionment factors, $g_{sc,i}$, are also applicable to humans a method for assigning measured TIA in humans to the relevant microscopic structures needed for alpha-emitter dosimetry is obtained. Specific adjustments for pharmacological or anatomical differences will improve the translation to human, i.e.: measuring fraction of occupancy in human cadavers to replace the murine based f_c values, would be a possible refinement of this basic approach. Furthermore, comparing $g_{sc,i}$ values measured in mice with those measured in a different non-human species such as dogs would help determine whether additional modifications such as scaling would need to be included.

Scope and Limitations

The macro to micro methodology presented is consistent with the MIRD absorbed fraction methodology; as such, the S-values calculated here are for a representative mouse or human. The nature of the macro to micro modeling approach precludes a calculation that is patient-specific since an ideal representative model of the relevant anatomy is used. The effect of anatomical variability in the patient or pre-clincial model can, however, be considered by parameter sensitivity analyses. Such an analysis is best performed for a specific radiopharmaceutical wherein the potential variability in pharmacokinetics and agent localization can also be considered. Such a study is not included in this initial description of macro to micro modeling. Extensions to account for the variation in number and size of glomeruli as a function of age (51), or to parameterize results as a function of kidney mass, could potentially be incorporated.

The pre-clinical measurements described in this work are based on morphological measurements derived from tissue sections, these are susceptible to potential sampling errors and shrinkage artifacts (55). The morphological parameter values obtained are in good agreement with published reports, however, and, an accounting of these second-order considerations was not undertaken.

Radiobiological Considerations

The purpose of dosimetry is to predict potential efficacy or toxicity, the extent to which the S-values provided in this work are dosimetrically useful depends upon the relationship between proximal tubule and/or glomerulus absorbed dose and renal failure. Since this level of analysis is unique to internally administered α-emitter-conjugated radiopharmaceuticals, human data to establish such a relationship are lacking. Pre-clinical studies, could, however address the question and, in fact, the work was motivated by pre-clinical work showing that renal cortex absorbed dose did not predict observed renal pathology in a pre-clinical model (4); this despite accounting for the higher energy deposition density of α-particles relative to β-particles which leads to a greater biological effect per unit absorbed dose. This “relative biological effectiveness” or RBE is on the order of 5 (24, 56, 57) and is likely to be cell type dependent.

Clearly, many questions remain and more work is required in α-particle dosimetry despite the headway made recently (25, 30–34). These questions raise the possibility that reliable α-particle renal dosimetry may lie outside of the realm of the MIRD absorbed fraction methodology, as has already proven to be the case for ^{223}Ra dosimetry of bone marrow (25). However, given the current level of assumptions in α-particle dosimetry, the model and results presented here represent a first step.

V. CONCLUSIONS

Alpha-particle therapy requires new models for dosimetry (24, 25). In the case of the kidney, the extension of the MIRD methodology to a microscopic level that can be linked to macroscopic measurements in humans will enable reliable α-particle dosimetry in radiopharmaceutical therapy and thereby help improve treatment implementation of targeted α-emitter therapy.

Acknowledgments

The authors would like to thank Dr. Catherine Foss for her assistance in the use of the Nikon microscope and software.

Financial support: NIH/NCI R01 CA157542, 2R01 CA116477.

REFERENCES

1. Imam SK. Advancements in cancer therapy with alpha-emitters: a review. IntJ RadiatOncol BiolPhys. 2001; 51(1):271–278.
2. McDevitt MR, Sgouros G, Finn RD, et al. Radioimmunotherapy with alpha-emitting nuclides. Eur J Nucl Med. 1998; 25(9):1341–1351. [PubMed: 9724387]
3. Friesen C, Glatting G, Koop B, et al. Breaking chemoresistance and radioresistance with [213Bi]anti-CD45 antibodies in leukemia cells. Cancer Res. 2007 Mar 1; 67(5):1950–1958. [PubMed: 17332322]
4. Song H, Hobbs RF, Vajravelu R, et al. Radioimmunotherapy of breast cancer metastases with alpha-particle emitter 225Ac: comparing efficacy with 213Bi and 90Y. Cancer Res. 2009 Dec 1; 69(23): 8941–8948. [PubMed: 19920193]
5. Song H, Shahverdi K, Huso DL, et al. 213Bi (alpha-emitter)-antibody targeting of breast cancer metastases in the neu-N transgenic mouse model. Cancer Res. 2008 May 15; 68(10):3873–3880. [PubMed: 18483272]
6. Lewington, VJ.; Parker, C.; Hindorf, C., et al. Alpharadin: A novel, targeted approach for treatment of bone metastases from CRPC-calculated alpha-particle dosimetry compared to a favorable clinical safety profile. ASCO Genitourinary Cancers Symposium; San Francisco, CA, USA. 2010.
7. Zalutsky MR, Bigner DD. Radioimmunotherapy with alpha-particle emitting radioimmunoconjugates. Acta Oncol. 1996; 35(3):373–379. [PubMed: 8679269]
8. Zalutsky MR, Reardon DA, Pozzi OR, Vaidyanathan G, Bigner DD. Targeted alpha-particle radiotherapy with 211At-labeled monoclonal antibodies. Nucl Med Biol. 2007 Oct; 34(7):779–785. [PubMed: 17921029]
9. McDevitt MR, Barendswaard E, Ma D, et al. An alpha-particle emitting antibody ([213Bi]J591) for radioimmunotherapy of prostate cancer. Cancer Res. 2000; 60(21):6095–6100. [PubMed: 11085533]
10. Sgouros G, Ballangrud AM, Jurcic JG, et al. Pharmacokinetics and dosimetry of an alpha-particle emitter labeled antibody: 213Bi-HuM195 (anti-CD33) in patients with leukemia. J Nucl Med. 1999; 40(11):1935–1946. [PubMed: 10565792]
11. Henriksen G, Breistol K, Bruland OS, Fodstad O, Larsen RH. Significant antitumor effect from bone-seeking, alpha-particle-emitting (223)Ra demonstrated in an experimental skeletal metastases model. Cancer Res. 2002 Jun 1; 62(11):3120–3125. [PubMed: 12036923]
12. Henriksen G, Fisher DR, Roeske JC, Bruland OS, Larsen RH. Targeting of osseous sites with alpha-emitting 223Ra: comparison with the beta-emitter 89Sr in mice. J Nucl Med. 2003 Feb; 44(2):252–259. [PubMed: 12571218]
13. Arazi L, Cooks T, Schmidt M, Keisari Y, Kelson I. The treatment of solid tumors by alpha emitters released from (224)Ra-loaded sources-internal dosimetry analysis. Phys Med Biol. 2010 Feb 21; 55(4):1203–1218. [PubMed: 20124656]
14. Andersson H, Cederkrantz E, Back T, et al. Intraperitoneal alpha-particle radioimmunotherapy of ovarian cancer patients: pharmacokinetics and dosimetry of (211)At-MX35 F(ab')2--a phase I study. J Nucl Med. 2009 Jul; 50(7):1153–1160. [PubMed: 19525452]
15. Zalutsky MR, Akabani G, Friedman HS, et al. Radioimmunotherapy of recurrent glioma patients using alpha-particle emitting astatine-211 labeled chimeric anti-tenascin monoclonal antibody. J Nucl Med. 2001; 42(5):121P–122P.
16. Zalutsky MR, Reardon DA, Akabani G, et al. Clinical Experience with {alpha}-Particle Emitting 211At: Treatment of Recurrent Brain Tumor Patients with 211At-Labeled Chimeric Antitenascin Monoclonal Antibody 81C6. J Nucl Med. 2008 Jan; 49(1):30–38. [PubMed: 18077533]
17. Jurcic JG, Larson SM, Sgouros G, et al. Targeted alpha-particle immunotherapy for myeloid leukemia. Blood. 2002; 100(4):1233–1239. [PubMed: 12149203]
18. Jurcic JG, McDevitt MR, Pandit-Taskar N, et al. Alpha-particle immunotherapy for acute myeloid leukemia (AML) with bismuth-213 and actinium-225. Cancer Biother Radiopharm. 2006; 21(4): 396–396.

19. Kneifel S, Cordier D, Good S, et al. Local targeting of malignant gliomas by the diffusible peptidic vector 1,4,7,10-tetraazacyclododecane-1-glutaric acid-4,7,10-triacetic acid-substance P. Clin Cancer Res. 2006; 12(12):3843–3850. [PubMed: 16778112]
20. Snyder, WS.; Ford, MR.; Warner, GG.; Watson, SB. "S," Absorbed Dose per Unit Cumulated Activity for Selected Radionuclides and Organs. MIRD Pamphlet No. 11. New York, NY, USA: Society of Nuclear Medicine; 1975.
21. Bolch WE, Eckerman KF, Sgouros G, Thomas SR. MIRD pamphlet No. 21: a generalized schema for radiopharmaceutical dosimetry--standardization of nomenclature. J Nucl Med. 2009 Mar; 50(3):477–484. [PubMed: 19258258]
22. Cristy, M.; Eckerman, K. Specific absorbed fractions of energy at various ages for internal photon sources. Oak Ridge, TN: Oak Ridge National Laboratory; 1987.
23. Bolch WE, Bouchet LG, Robertson JS, et al. MIRD pamphlet No. 17: the dosimetry of nonuniform activity distributions--radionuclide S values at the voxel level. Medical Internal Radiation Dose Committee. J Nucl Med. 1999; 40(1):11S–36S. [PubMed: 9935083]
24. Sgouros G, Roeske JC, McDevitt MR, et al. MIRD Pamphlet No. 22 (abridged): radiobiology and dosimetry of alpha-particle emitters for targeted radionuclide therapy. J Nucl Med. 2010 Feb; 51(2):311–328. [PubMed: 20080889]
25. Hobbs R, Song H, Watchman CJ, et al. Bone marrow toxicity considerations from 223Ra radiopharmaceutical therapy. Eur J Nucl Med Mol Imaging. 2011 *(submitted to)*.
26. Akabani G, Kennel SJ, Zalutsky MR. Microdosimetric analysis of alpha-particle-emitting targeted radiotherapeutics using histological images. J Nucl Med. 2003; 44(5):792–805. [PubMed: 12732682]
27. Akabani G, Zalutsky MR. Microdosimetry of astatine-211 using histological images: application to bone marrow. Radiat Res. 1997; 148(6):599–607. [PubMed: 9399706]
28. Aurlien E, Larsen RH, Akabani G, Olsen DR, Zalutsky MR, Bruland OS. Exposure of human osteosarcoma and bone marrow cells to tumour-targeted alpha-particles and gamma-irradiation: analysis of cell survival and microdosimetry. Int J Radiat Biol. 2000 Aug; 76(8):1129–1141. [PubMed: 10947126]
29. Larsson E, Meerkhan SA, Strand SE, Jonsson BA. A small-scale anatomic model for testicular radiation dosimetry for radionuclides localized in the human testes. J Nucl Med. 2011 Jan; 53(1): 72–81. [PubMed: 22080442]
30. Jaggi JS, Seshan SV, McDevitt MR, LaPerle K, Sgouros G, Scheinberg DA. Renal tubulointerstitial changes after internal irradiation with alpha-particle-emitting actinium daughters. J Am Soc Nephrol. 2005 Sep; 16(9):2677–2689. [PubMed: 15987754]
31. Jaggi JS, Seshan SV, McDevitt MR, Sgouros G, Hyjek E, Scheinberg DA. Mitigation of radiation nephropathy after internal alpha-particle irradiation of kidneys. Int J Radiat Oncol Biol Phys. 2006 Apr 1; 64(5):1503–1512. [PubMed: 16503385]
32. Schwartz J, Jaggi JS, O'Donoghue JA, et al. Renal uptake of bismuth-213 and its contribution to kidney radiation dose following administration of actinium-225-labeled antibody. Phys Med Biol. 2011 Feb 7; 56(3):721–733. [PubMed: 21220845]
33. Back T, Haraldsson B, Hultborn R, et al. Glomerular filtration rate after alpha-radioimmunotherapy with 211At-MX35-F(ab')2: a long-term study of renal function in nude mice. Cancer Biother Radiopharm. 2009 Dec; 24(6):649–658. [PubMed: 20025544]
34. Back T, Jacobsson L. The alpha-camera: a quantitative digital autoradiography technique using a charge-coupled device for ex vivo high-resolution bioimaging of alpha-particles. J Nucl Med. 2010 Oct; 51(10):1616–1623. [PubMed: 20847171]
35. Nyengaard JR, Bendtsen TF. Glomerular number and size in relation to age, kidney weight, and body surface in normal man. Anat Rec. 1992 Feb; 232(2):194–201. [PubMed: 1546799]
36. Agostinelli S, Allison J, Amako K, et al. GEANT4 - a simulation toolkit. Nucl. Instum. Methods Phys. Res. A. 2003; 506:250–303.
37. Hobbs RF, Baechler S, Wahl RL, et al. Arterial wall dosimetry for non-Hodgkin lymphoma patients treated with radioimmunotherapy. J Nucl Med. 2010 Mar; 51(3):368–375. [PubMed: 20150265]

38. Hobbs R, Baechler S, Fu DX, et al. A model of cellular dosimetry for macroscopic tumors in radiopharmaceutical therapy. Med Phys. 2011; 38(6):2892–2903. [PubMed: 21815364]
39. Chouin N, Bernardeau K, Bardies M, et al. Evidence of extranuclear cell sensitivity to alpha-particle radiation using a microdosimetric model. II. Application of the microdosimetric model to experimental results. Radiat Res. 2009 Jun; 171(6):664–673. [PubMed: 19580473]
40. Chouin N, Bernardeau K, Davodeau F, et al. Evidence of extranuclear cell sensitivity to alpha-particle radiation using a microdosimetric model. I. Presentation and validation of a microdosimetric model. Radiat Res. 2009 Jun; 171(6):657–663. [PubMed: 19580472]
41. Russ GA, Bigler RE, Tilbury RS, Woodard HQ, Laughlin JS. Metabolic studies with radiobismuth. I. Retention and distribution of 206Bi in the normal rat. Radiat Res. 1975 Sep; 63(3):443–454. [PubMed: 1162032]
42. Jaggi JS, Kappel BJ, McDevitt MR, et al. Efforts to control the errant products of a targeted in vivo generator. Cancer Res. 2005 Jun 1; 65(11):4888–4895. [PubMed: 15930310]
43. Chu S, Ekström L, Firestone R. WWW Table of Radioactive Isotopes. http://nucleardata.nuclear.lu.se/nucleardata/toi/.
44. Bouchet LG, Bolch WE, Blanco HP, et al. MIRD Pamphlet No 19: absorbed fractions and radionuclide S values for six age-dependent multiregion models of the kidney. J Nucl Med. 2003; 44(7):1113–1147. [PubMed: 12843230]
45. Stabin MG, Sparks RB, Crowe E. OLINDA/EXM: the second-generation personal computer software for internal dose assessment in nuclear medicine. J Nucl Med. 2005 Jun; 46(6):1023–1027. [PubMed: 15937315]
46. Loevinger, R.; Budinger, TF.; Watson, EE. MIRD Primer for Absorbed Dose Calculations. New York, NY, USA: The Society of Nuclear Medicine, Inc.; 1991.
47. Brindle JM, Trindade AA, Pichardo JC, Myers SL, Shah AP, Bolch WE. CT volumetry of the skeletal tissues. Med Phys. 2006 Oct; 33(10):3796–3803. [PubMed: 17089844]
48. De Jong M, Valkema R, Van Gameren A, et al. Inhomogeneous localization of radioactivity in the human kidney after injection of [(111)In-DTPA]octreotide. J Nucl Med. 2004 Jul; 45(7):1168–1171. [PubMed: 15235063]
49. Bhathena DB. Glomerular size and the association of focal glomerulosclerosis in long-surviving human renal allografts. J Am Soc Nephrol. 1993 Dec; 4(6):1316–1326. [PubMed: 8130358]
50. Taketo M, Schroeder AC, Mobraaten LE, et al. FVB/N: an inbred mouse strain preferable for transgenic analyses. Proc Natl Acad Sci U S A. 1991 Mar 15; 88(6):2065–2069. [PubMed: 1848692]
51. Sato F, Tsuchihashi S, Kawashima N. Age changes in number and size of the murine renal glomeruli. Exp Gerontol. 1975; 10(6):325–331. [PubMed: 1213044]
52. Barone R, Borson-Chazot F, Valkema R, et al. Patient-specific dosimetry in predicting renal toxicity with (90)Y-DOTATOC: relevance of kidney volume and dose rate in finding a dose-effect relationship. J Nucl Med. 2005 Jan; 46(Suppl 1):99S–106S. [PubMed: 15653658]
53. Wessels BW, Konijnenberg MW, Dale RG, et al. MIRD pamphlet No. 20: the effect of model assumptions on kidney dosimetry and response--implications for radionuclide therapy. J Nucl Med. 2008 Nov; 49(11):1884–1899. [PubMed: 18927342]
54. Jamison RL. Intrarenal heterogeneity. The case for two functionally dissimilar populations of nephrons in the mammalian kidney. Am J Med. 1973 Mar; 54(3):281–289. [PubMed: 4571744]
55. Dorph-Petersen KA, Nyengaard JR, Gundersen HJ. Tissue shrinkage and unbiased stereological estimation of particle number and size. J Microsc. 2001 Dec; 204(Pt 3):232–246. [PubMed: 11903800]
56. Behr TM, Behe M, Sgouros G. Correlation of red marrow radiation dosimetry with myelotoxicity: empirical factors influencing the radiation-induced myelotoxicity of radiolabeled antibodies, fragments and peptides in pre-clinical and clinical settings. Cancer Biother Radiopharm. 2002; 17(4):445–464. [PubMed: 12396708]
57. Dahle J, Bruland OS, Larsen RH. Relative biologic effects of low-dose-rate alpha-emitting 227Th-rituximab and beta-emitting 90Y-tiuexetan-ibritumomab versus external beam X-radiation. Int J Radiat Oncol Biol Phys. 2008 Sep 1; 72(1):186–192. [PubMed: 18722269]

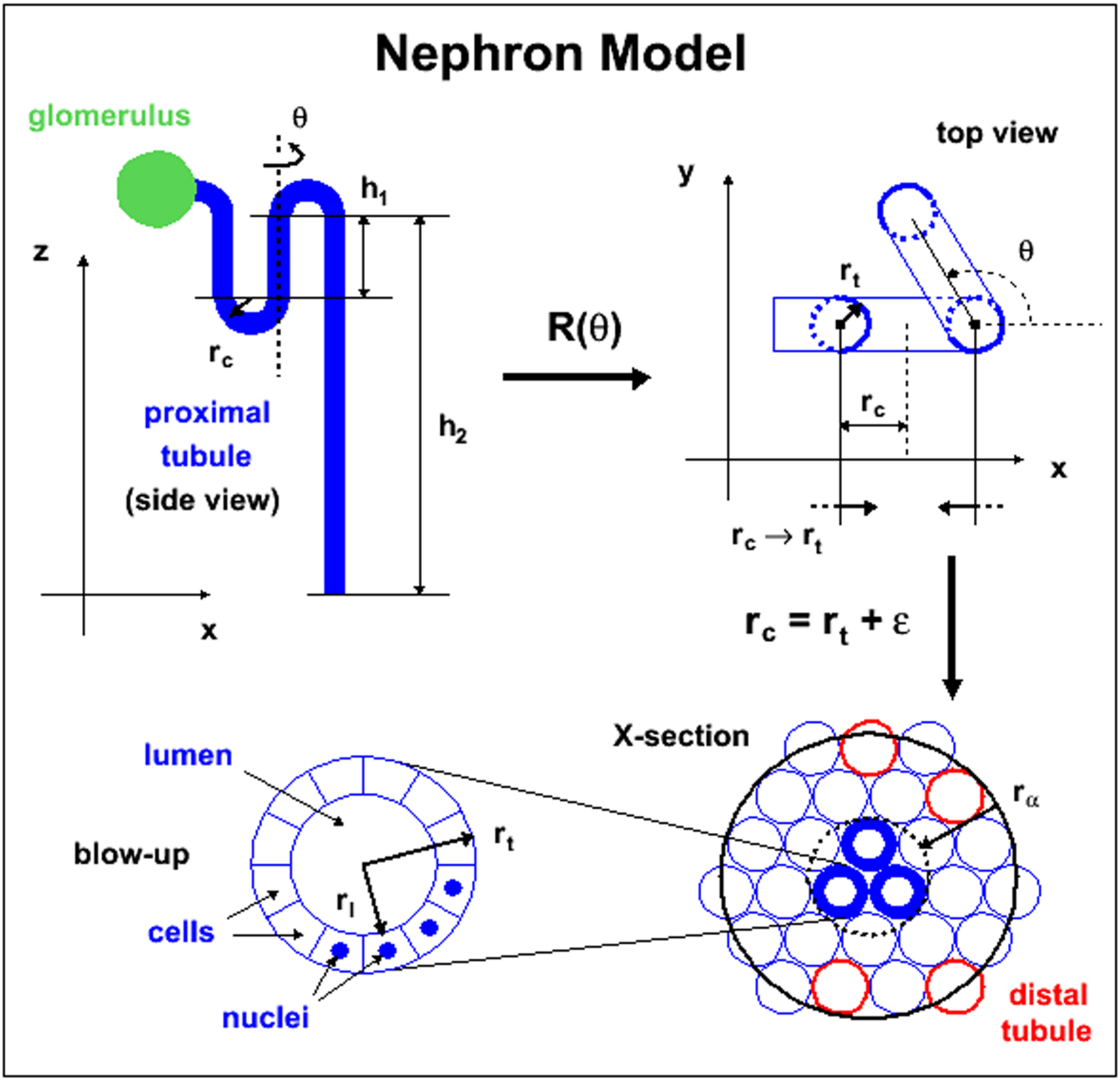

Figure 1.

Idealized geometrical nephron model. The parameters shown are those used for the simulation: r_t is the proximal tubule radius, r_l is the lumen radius as measured by histology. The ε value is taken to be 1μm and corresponds to interstitial space, h_1 and h_2 represent the scale of the proximal tubule length.

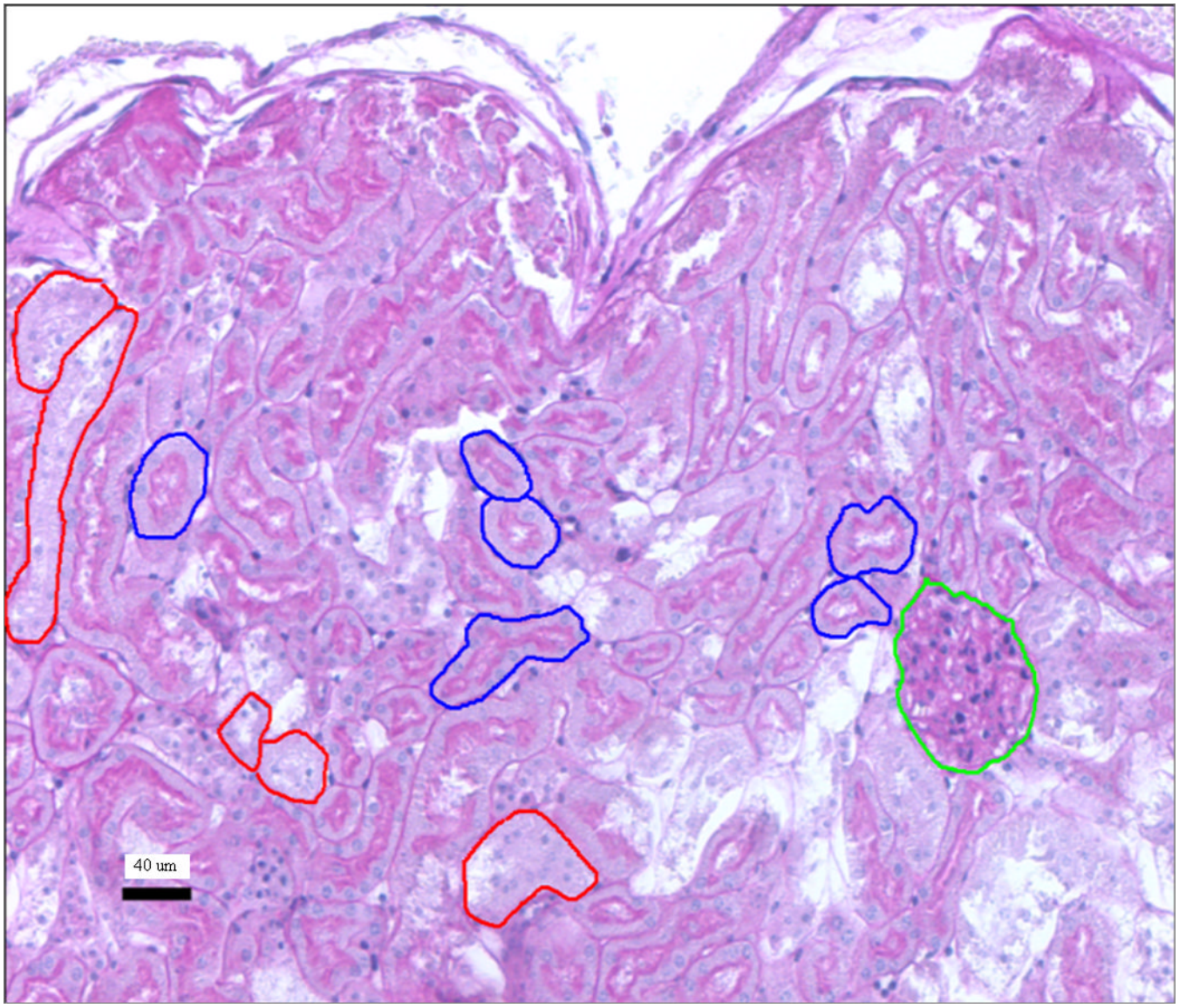

Figure 2.
Murine histological sample stained with PAS. The different compartments are contoured in different colors: the glomeruli (glc) in green, the proximal tubules in blue and the distal tubules in red.

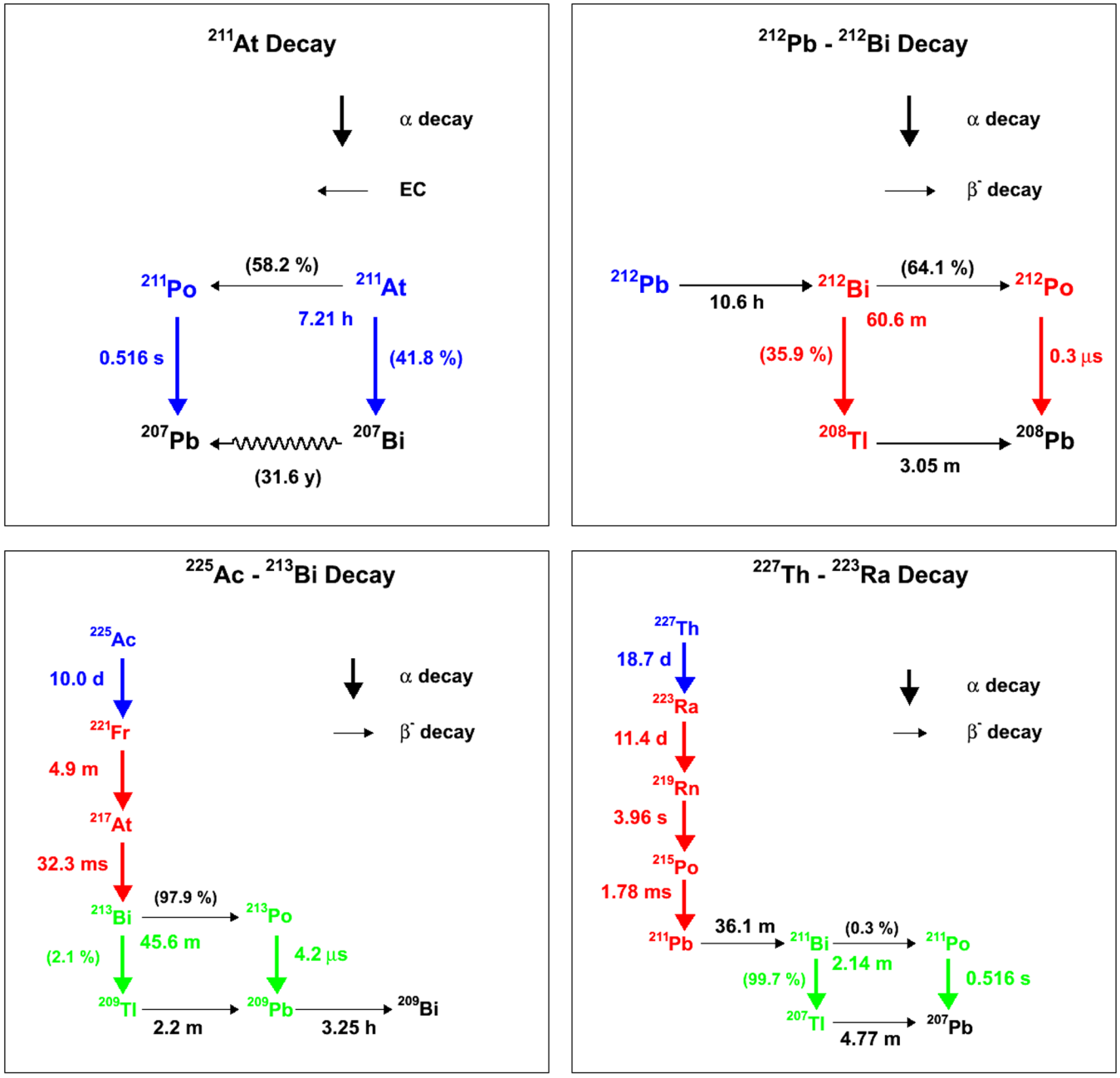

Figure 3.

Decay schemes for currently used α-emitting radiopharmaceuticals. Within each figure, the decays shown in a same color are considered as a single S-value because of the short half-life of the descendants. In figure 3a, the long half-life of ^{207}Bi precludes it from contributing to therapeutic absorbed dose and is thus represented as a squiggly line.

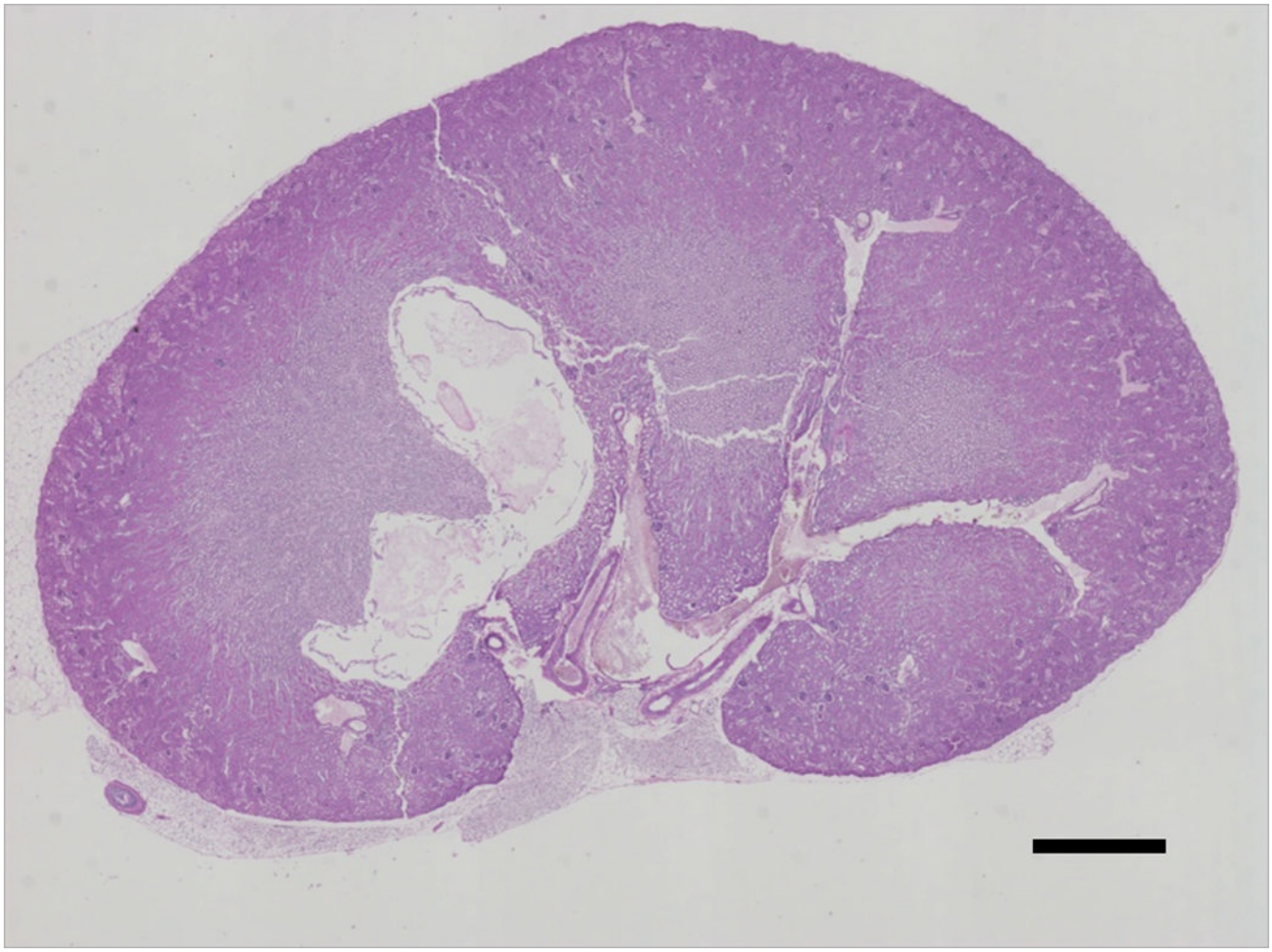

Figure 4.
Whole kidney slice established by stitching individual images in the Nikon Elements BL software. From such images, representative smaller regions were delineated and contours were drawn on the different compartments and source regions to determine fractions of occupancy as well as nephron component parameter sizes. The scale bar is 1 mm long.

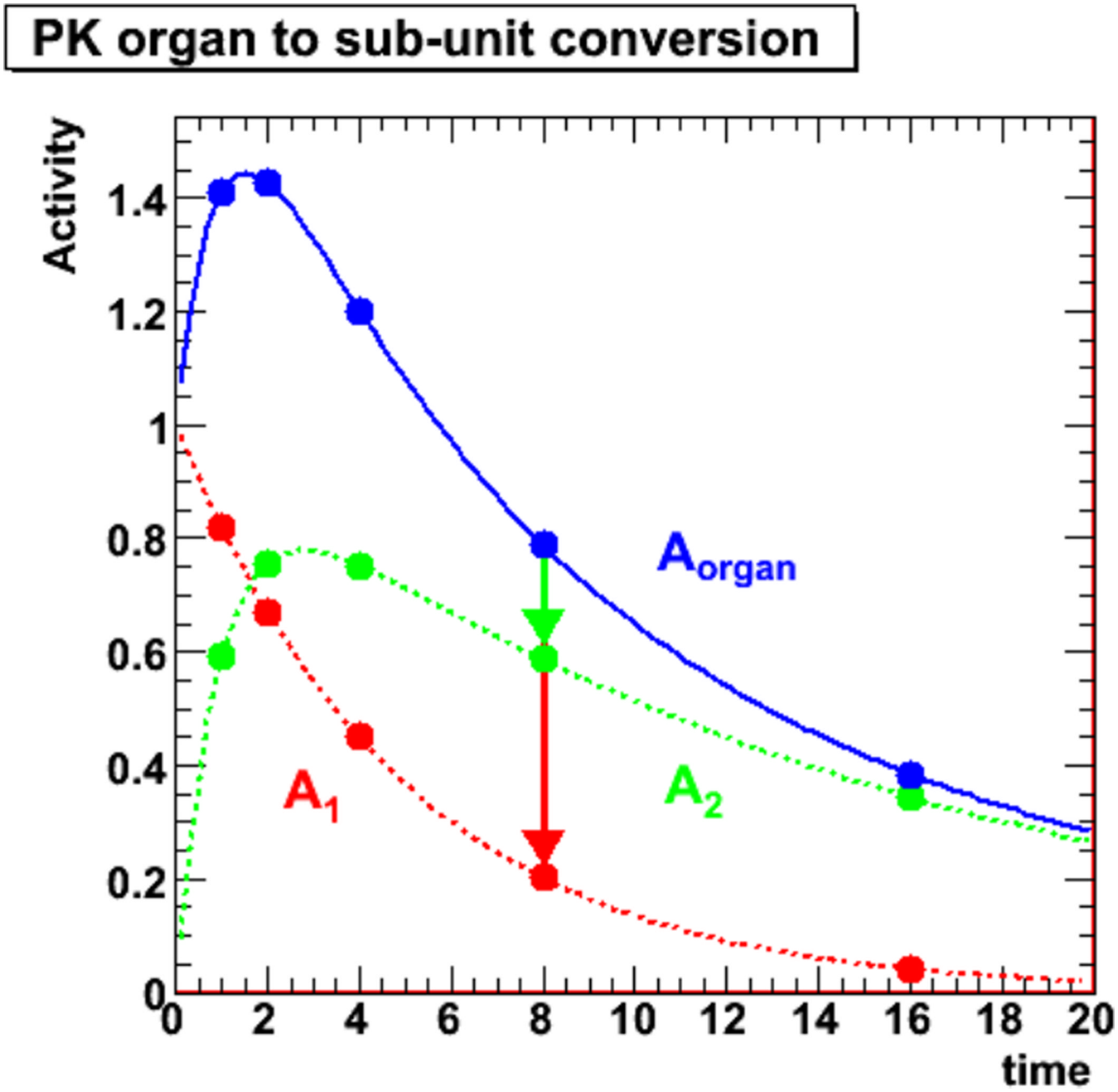

Figure 5.
Illustration of pharmacokinetics of an idealized 2-compartment system (kidney or cortex), which represents the total activity in the kidney at each time point as the sum of the activities in the two compartments A_1 and A_2 (proximal tubules and glomeruli). Note that the units of activity and time are arbitrary.

Phys Med Biol. Author manuscript; available in PMC 2013 May 01.

Table I

Table I: decay schemes and energies for α-emitters used in RPT. These tables correspond to the decay schemes illustrated in figure 1. Table Ia is for the ^{211}At decay chain, table Ib for ^{212}Pb, table Ic for ^{225}Ac and table Id for ^{227}Th.

Table	isotope	decay	energy (MeV)	branching ratio	half-life	descendant
Ia	^{211}At	alpha	5.98	0.418	7.21 h	^{207}Po
	^{211}At	EC	-	0.582	7.21 h	^{211}Po
	^{211}Po	alpha	7.59	1.000	0.516 s	^{207}Pb
Ib	^{212}Pb	beta	0.102	1.000	10.6 h	^{212}Bi
	^{212}Bi	alpha	6.21	0.359	60.6 min	^{208}Tl
	^{212}Bi	beta	0.774	0.641	60.6 min	^{212}Po
	^{212}Po	alpha	8.95	1.000	0.3 us	^{208}Pb
	^{208}Tl	beta	0.558	1.000	3.05 min	^{208}Pb
Ic	^{225}Ac	alpha	5.95	1.000	10.0 d	^{221}Fr
	^{221}Fr	alpha	6.46	1.000	4.9 min	^{217}At
	^{217}At	alpha	7.2	1.000	32.3 ms	^{213}Bi
	^{213}Bi	alpha	5.98	0.021	45.6 min	^{209}Tl
	^{213}Bi	Beta	0.428	0.979	45.6 min	^{213}Po
	^{213}Po	Alpha	8.54	1.000	4.2 us	^{209}Pb
	^{209}Tl	Beta	0.659	1.000	2.2 min	^{209}Pb
	^{209}Pb	Beta	0.193	1.000	3.25 h	^{209}Bi
Id	^{227}Th	Alpha	6.15	1.000	18.7 d	^{223}Ra
	^{223}Ra	Alpha	5.98	1.000	11.4 d	^{219}Rn
	^{219}Rn	Alpha	6.95	1.000	3.96 s	^{215}Po
	^{215}Po	Alpha	7.53	1.000	1.78 ms	^{211}Pb
	^{211}Pb	Beta	0.449	1.000	36.1 min	^{211}Bi
	^{211}Bi	Alpha	6.75	0.997	2.14 min	^{211}Po
	^{211}Bi	Beta	-	0.003	2.14 min	^{207}Tl
	^{211}Po	Alpha	7.59	1.000	0.516 s	^{207}Pb

Table	isotope	decay	energy (MeV)	branching ratio	half-life	descendant
	^{207}Tl	Beta	0.495	1.000	4.77 min	^{207}Pb

Table II

Tables II: α-particle murine S-values for the nephron model and associated values. The (u) indicates the Monte Carlo results for the single unit nephron geometrical model, while the (c) values are the compartmental S-values to be used when applying the model and are derived from the unit values using equation (4). The percentage (%) column shows the percentage of emitted energy from the source that is absorbed in the target. Nephron S values for glomerular cells “glc”, proximal tubule cells “prtc”, the proximal tubule lumen “prtl”, the proximal tubule lumen surface “prts”, and the prximal tubule as a single compartment “prt” are listed. The kidney compartments are the kidney “kid” and the cortex “cor”. Table IIa is for the ^{211}At decay chain, table IIb is for ^{212}Bi, table IIc is for ^{225}Ac, table IId is for ^{221}Fr (including^{217}At), table IIe is for ^{213}Bi, table IIf is for ^{227}Th, table IIg is for ^{223}Ra (including ^{219}Rn and ^{215}Po), table IIh is for ^{211}Bi. Note that the slightly higher than 100 % values for some kidney self-dose S-values reflects the minor discrepancies between theoretical and GEANT4 modeled energy deposition (less than 1 %).

a

^{211}At	S-value (u) (Gy/Bq-s)	Absorbed Energy (MeV/decay)	%	S-value (c) (Gy/Bq-s)
glc←glc	5.90E-04	4.41	63.76	1.58E-07
glc←prt	2.29E-04	1.71	24.73	2.13E-09
prtc←glc	2.81E-04	0.06	0.91	2.24E-09
prtc←prtc	7.85E-04	5.02	72.63	6.26E-09
prtc←prtl	7.85E-04	5.03	72.67	6.26E-09
prtc←prts	7.87E-04	5.04	72.83	6.28E-09
kid←kid	-	6.94	100.33	3.76E-09
cor←cor	-	6.16	89.00	5.07E-09

b

^{212}Bi	S-value (u) (Gy/Bq-s)	Absorbed Energy (MeV/decay)	%	S-value (c) (Gy/Bq-s)
glc←glc	5.71E-04	4.27	53.60	1.53E-07
glc←prt	1.14E-05	2.44	30.59	3.04E-09
prtc←glc	3.63E-04	0.08	1.02	2.90E-09
prtc←prtc	9.27E-04	5.94	74.51	7.39E-09
prtc←prtl	9.28E-04	5.94	74.58	7.40E-09
prtc←prts	9.27E-04	5.93	74.48	7.39E-09
kid←kid	-	7.9	99.17	4.28E-09
cor←cor	-	6.94	87.12	5.71E-09

c

^{225}Ac	S-value (u) (Gy/Bq-s)	Absorbed Energy (MeV/decay)	%	S-value (c) (Gy/Bq-s)
glc←glc	5.74E-04	4.29	72.10	1.53E-07
glc←prt	5.20E-06	1.12	18.76	1.39E-09
prtc←glc	2.33E-04	0.05	0.87	1.86E-09
prtc←prtc	6.82E-04	4.37	73.39	5.44E-09

c

^{225}Ac	S-value (u) (Gy/Bq-s)	Absorbed Energy (MeV/decay)	%	S-value (c) (Gy/Bq-s)
prtc←prtl	6.85E-04	4.39	73.70	5.46E-09
prtc←prts	6.84E-04	4.38	73.57	5.45E-09
kid←kid	-	5.94	99.83	3.22E-09
cor←cor	-	5.40	90.76	4.44E-09

d

^{221}Fr (incl. ^{217}At)	S-value (u) (Gy/Bq-s)	Absorbed Energy (MeV/decay)	%	S-value (c) (Gy/Bq-s)
glc←glc	1.19E-03	8.88	65.01	3.18E-07
glc←prt	1.51E-05	3.25	23.79	4.05E-09
prtc←glc	5.60E-04	0.12	0.91	4.47E-09
prtc←prtc	1.55E-03	9.92	72.64	1.24E-08
prtc←prtl	1.55E-03	9.93	72.70	1.24E-08
prtc←prts	1.55E-03	9.92	72.62	1.24E-08
kid←kid	-	13.7	100.29	7.42E-09
cor←cor	-	12.20	89.31	1.00E-08

e

^{213}Bi	S-value (u) (Gy/Bq-s)	Absorbed Energy (MeV/decay)	%	S-value (c) (Gy/Bq-s)
glc←glc	5.88E-04	4.4	51.85	1.57E-07
glc←prt	1.27E-05	2.73	32.22	3.41E-09
prtc←glc	4.03E-04	0.09	1.06	3.21E-09
prtc←prtc	9.34E-04	5.98	70.43	7.45E-09
prtc←prtl	9.36E-04	5.99	70.57	7.46E-09
prtc←prts	9.38E-04	6.01	70.78	7.48E-09
kid←kid	-	8.43	99.34	4.57E-09
cor←cor	-	7.36	86.73	6.06E-09

f

^{227}Th	S-value (u) (Gy/Bq-s)	Absorbed Energy (MeV/decay)	%	S-value (c) (Gy/Bq-s)
glc←glc	5.79E-04	4.33	70.41	1.55E-07
glc←prt	5.38E-06	1.16	18.79	1.44E-09
prtc←glc	2.48E-04	0.06	0.90	1.98E-09
prtc←prtc	6.99E-04	4.47	72.74	5.57E-09
prtc←prtl	7.01E-04	4.49	73.01	5.59E-09
prtc←prts	6.98E-04	4.47	72.70	5.57E-09
kid←kid	-	6.03	98.05	3.27E-09

f

^{227}Th	S-value (u) (Gy/Bq-s)	Absorbed Energy (MeV/decay)	%	S-value (c) (Gy/Bq-s)
cor←cor	-	5.48	89.11	4.51E-09

g

^{223}Ra (incl.^{219}Rn,^{215}Po)	S-value (u) (Gy/Bq-s)	Absorbed Energy (MeV/decay)	%	S-value (c) (Gy/Bq-s)
glc←glc	1.78E-03	13.3	65.00	4.76E-07
glc←prt	2.20E-05	4.72	23.08	5.88E-09
prtc←glc	8.61E-04	0.19	0.94	6.87E-09
prtc←prtc	2.31E-03	14.77	72.17	1.84E-08
prtc←prtl	2.31E-03	14.80	72.33	1.84E-08
prtc←prts	2.31E-03	14.80	72.33	1.84E-08
kid←kid	-	20.3	99.22	1.10E-08
cor←cor	-	18.10	88.47	1.49E-08

h

^{211}Bi	S-value (u) (Gy/Bq-s)	Absorbed Energy (MeV/decay)	%	S-value (c) (Gy/Bq-s)
glc←glc	5.94E-04	4.44	65.75	1.59E-07
glc←prt	7.23E-06	1.55	22.99	1.93E-09
prtc←glc	2.77E-04	0.06	0.91	2.21E-09
prtc←prtc	7.64E-04	4.89	72.47	6.10E-09
prtc←prtl	7.65E-04	4.90	72.56	6.10E-09
prtc←prts	7.66E-04	4.90	72.60	6.11E-09
kid←kid	-	6.73	99.67	3.65E-09
cor←cor	-	5.99	88.71	4.93E-09

Table III

Tables III: human S-values for the nephron model and associated values. The tables correspond to the same respective radionuclides and compartments as for tables II. The S-values for the kidney and cortex are included for completeness; they were calculated assuming that 100 % of the alpha energy is absorbed in both cases.

a

^{211}At	S-value (u) (Gy/Bq-s)	Absorbed Energy (MeV/decay)	%	S-value (c) (Gy/Bq-s)
glc←glc	6.37E-05	5.85	84.57	2.06E-10
glc←prt	8.34E-06	1.16	16.77	9.40E-13
prtc←glc	3.44E-05	0.157	2.27	3.55E-12
prtc←prtc	5.27E-05	1.54	22.26	5.44E-12
prtc←prtl	5.23E-05	1.95	28.19	5.40E-12
prtc←prts	5.25E-05	1.77	25.59	5.42E-12
kid←kid	-	6.92	100	3.69E-12
cor←cor	-	6.92	100	5.60E-12

b

^{212}Bi	S-value (u) (Gy/Bq-s)	Absorbed Energy (MeV/decay)	%	S-value (c) (Gy/Bq-s)
glc←glc	6.87E-05	6.31	79.21	2.22E-10
glc←prt	1.25E-05	1.74	21.84	1.41E-12
prtc←glc	3.93E-05	0.234	2.94	4.06E-12
prtc←prtc	6.07E-05	1.8	22.60	6.27E-12
prtc←prtl	6.04E-05	2.11	26.49	6.23E-12
prtc←prts	6.05E-05	1.98	24.85	6.25E-12
kid←kid	-	7.97	100	4.25E-12
cor←cor	-	7.97	100	6.45E-12

c

^{225}Ac	S-value (u) (Gy/Bq-s)	Absorbed Energy (MeV/decay)	%	S-value (c) (Gy/Bq-s)
glc←glc	5.70E-05	5.24	88.07	1.85E-10
glc←prt	5.39E-06	0.75	12.61	6.08E-13
prtc←glc	3.02E-05	0.096	1.61	3.12E-12
prtc←prtc	4.54E-05	1.28	21.51	4.69E-12
prtc←prtl	4.49E-05	1.76	29.58	4.64E-12
prtc←prts	4.52E-05	1.53	25.71	4.66E-12
kid←kid	-	5.95	100.00	3.17E-12
cor←cor	-	5.95	100.00	4.82E-12

d

^{221}Fr (incl. ^{217}At)	S-value (u) (Gy/Bq-s)	Absorbed Energy (MeV/decay)	%	S-value (c) (Gy/Bq-s)
glc←glc	1.26E-04	11.6	84.92	4.09E-10
glc←prt	1.57E-05	2.19	16.03	1.77E-12
prtc←glc	6.91E-05	0.302	2.21	7.13E-12
prtc←prtc	1.04E-04	2.96	21.67	1.08E-11
prtc←prtl	1.03E-04	3.84	28.11	1.07E-11
prtc←prts	1.04E-04	3.48	25.48	1.07E-11
kid←kid	-	13.66	100.00	7.29E-12
cor←cor	-	13.66	100.00	1.11E-11

e

^{213}Bi	S-value (u) (Gy/Bq-s)	Absorbed Energy (MeV/decay)	%	S-value (c) (Gy/Bq-s)
glc←glc	7.28E-05	6.69	78.83	2.36E-10
glc←prt	1.36E-05	1.89	22.27	1.53E-12
prtc←glc	4.22E-05	0.266	3.13	4.36E-12
prtc←prtc	6.47E-05	1.89	22.27	6.68E-12
prtc←prtl	6.45E-05	2.1	24.75	6.65E-12
prtc←prts	6.46E-05	2.03	23.92	6.66E-12
kid←kid	-	8.49	100.00	4.53E-12
cor←cor	-	8.49	100.00	6.87E-12

f

^{227}Th	S-value (u) (Gy/Bq-s)	Absorbed Energy (MeV/decay)	%	S-value (c) (Gy/Bq-s)
glc←glc	5.78E-05	5.31	86.34	1.87E-10
glc←prt	5.55E-06	0.772	12.55	6.25E-13
prtc←glc	3.16E-05	0.098	1.59	3.26E-12
prtc←prtc	4.70E-05	1.29	20.98	4.85E-12
prtc←prtl	4.65E-05	1.79	29.11	4.79E-12
prtc←prts	4.67E-05	1.57	25.53	4.82E-12
kid←kid	-	6.15	100.00	3.28E-12
cor←cor	-	6.15	100.00	4.98E-12

g

^{223}Ra (incl.^{219}Rn,^{215}Po)	S-value (u) (Gy/Bq-s)	Absorbed Energy (MeV/decay)	%	S-value (c) (Gy/Bq-s)
glc←glc	1.87E-04	17.2	84.07	6.06E-10
glc←prt	2.32E-05	3.23	15.79	2.62E-12
prtc←glc	1.04E-04	0.415	2.03	1.08E-11
prtc←prtc	1.56E-04	4.37	21.36	1.61E-11

g

^{223}Ra (incl.^{219}Rn,^{215}Po)	S-value (u) (Gy/Bq-s)	Absorbed Energy (MeV/decay)	%	S-value (c) (Gy/Bq-s)
prtc←prtl	1.55E-04	5.83	28.49	1.60E-11
prtc←prts	1.55E-04	5.08	24.83	1.60E-11
kid←kid	-	20.46	100.00	1.09E-11
cor←cor	-	20.46	100.00	1.66E-11

h

^{211}Bi	S-value (u) (Gy/Bq-s)	Absorbed Energy (MeV/decay)	%	S-value (c) (Gy/Bq-s)
glc←glc	6.27E-05	5.76	85.30	2.03E-10
glc←prt	7.33E-06	1.02	15.11	8.26E-13
prtc←glc	3.40E-05	0.145	2.15	3.51E-12
prtc←prtc	5.15E-05	1.47	21.77	5.32E-12
prtc←prtl	5.11E-05	1.89	27.99	5.27E-12
prtc←prts	5.12E-05	1.74	25.77	5.29E-12
kid←kid	-	6.75	100.00	3.60E-12
cor←cor	-	6.75	100.00	5.47E-12

Table IV

Tables IV: β-decay murine S-values for the nephron model and associated values. Table IIa is for the ^{212}Bi decay chain, table IVb is for the ^{225}Ac chain, table IVc is for the ^{227}Th decay chain.

a

Isotope		Absorbed Energy (MeV/decay)	%	S-value (Gy/Bq-s)
^{212}Pb	kid←kid	0.0937	91.86	5.08E-11
	cor←cor	0.0869	85.20	7.15E-11
^{212}Bi	kid←kid	0.357	46.12	1.93E-10
	cor←cor	0.166	21.45	1.37E-10
^{208}Tl	kid←kid	0.323	57.89	1.75E-10
	cor←cor	0.234	41.94	1.93E-10

b

Isotope		Absorbed Energy (MeV/decay)	%	S-value (Gy/Bq-s)
^{213}Bi	kid←kid	0.284	66.36	1.54E-10
	cor←cor	0.208	48.60	1.71E-10
^{209}Tl	kid←kid	0.34	51.59	1.84E-10
	cor←cor	0.246	37.33	2.02E-10
^{209}Pb	kid←kid	0.17	88.08	9.21E-11
	cor←cor	0.145	75.13	1.19E-10

c

Isotope		Absorbed Energy (MeV/decay)	%	S-value (Gy/Bq-s)
^{211}Pb	kid←kid	0.295	65.70	1.60E-10
	cor←cor	0.22	49.00	1.81E-10
^{207}Tl	kid←kid	0.309	62.42	1.67E-10
	cor←cor	0.228	46.06	1.88E-10